Experimental characterization of graphene by electrostatic resonance frequency tuning

Sajadi, Banafsheh; Alijani, Farbod; Davidovikj, Dejan; Goosen, Hans; Steeneken, Peter; van Keulen, Fred

Important note
To cite this publication, please use the final published version (if applicable).
Please check the document version above.

Experimental characterization of graphene by electrostatic resonance frequency tuning

Banafsheh Sajadi, Farbod Alijani, Dejan Davidovikj, Johannes (Hans) Goosen, Peter G. Steeneken, and Fred van Keulen

Articles you may be interested in

Graphene membrane dynamics provides a noncontact alternative for material characterization
Scilight **2017**, 260003 (2017); 10.1063/1.5019686

Thermoreflectance microscopy measurements of the Joule heating characteristics of high-T_c superconducting terahertz emitters
Journal of Applied Physics **122**, 233902 (2017); 10.1063/1.5002743

Chaos: The speed limiting phenomenon in dynamic atomic force microscopy
Journal of Applied Physics **122**, 224306 (2017); 10.1063/1.5000130

Wavefront modulation and controlling for Lamb waves using surface bonded slice lenses
Journal of Applied Physics **122**, 234902 (2017); 10.1063/1.4999627

Perspective: Terahertz science and technology
Journal of Applied Physics **122**, 230901 (2017); 10.1063/1.5007683

Determination of electrical properties of degraded mixed ionic conductors: Impedance studies with applied dc voltage
Journal of Applied Physics **122**, 244101 (2017); 10.1063/1.5006062

Experimental characterization of graphene by electrostatic resonance frequency tuning

Banafsheh Sajadi,[1] Farbod Alijani,[1,a)] Dejan Davidovikj,[2] Johannes (Hans) Goosen,[1] Peter G. Steeneken,[1,2] and Fred van Keulen[1]

[1]*Department of Precision and Microsystem Engineering, Delft University of Technology, 2628 CD Delft, The Netherlands*
[2]*Kavli Institute of Nanoscience, Delft University of Technology, 2628 CJ Delft, The Netherlands*

In the last decade, graphene membranes have drawn tremendous attention due to their potential application in Nano-Electro-Mechanical Systems. In this paper, we show that the frequency response curves of graphene resonators are powerful tools for their dynamic characterization and for extracting their equivalent Young's modulus. For this purpose, vibrations of an electrostatically actuated circular graphene membrane are studied both experimentally and numerically. The experiments reveal the dependency of the linear and nonlinear resonance frequency of the nano-resonator on the driving DC and AC voltages. A numerical model is proposed based on the nonlinear membrane theory, and by fitting the numerically calculated change in resonance frequency due to the DC voltage to those of the experimental observations, the Young's modulus is determined. It is shown that by using the obtained equivalent Young's modulus, the numerical model can accurately describe the nonlinear dynamics of the graphene membrane in other sets of measurements. *Published by AIP Publishing.*
https://doi.org/10.1063/1.4999682

I. INTRODUCTION

The exceptional mechanical properties of graphene have made it a promising candidate for the next generation of two dimensional (2D) nano-resonators. Potential applications of these resonators are, among others, pressure, gas, and mass sensors.[1–5] In this class, *electrostatically actuated* 2D-nano-resonators have a superior advantage for the potential integration and packaging in commercial Nano-Electro-Mechanical Systems (NEMS).[6–10] In these devices, typically, a parallel-plate capacitor is formed between a fixed bottom electrode and a suspended flexible single or multi-layer graphene membrane. When an alternating (AC) electric potential is applied, a dynamic attractive electrostatic load is induced between the electrodes, leading to the deformation and high-frequency excitation of the membrane. In this work, a methodology is outlined in which the dependency of the resonance frequency on the DC voltage is used to determine the mechanical properties of the graphene membrane.

The conventional method for determining the mechanical properties of suspended 2D-materials is Atomic Force Microscopy (AFM).[11] Based on AFM measurements, a large range of elastic moduli (0.1–1.1 TPa) has been reported for suspended graphene ribbons and drums.[12–14] AFM requires mechanical contact between a sharp tip and the membrane, which might potentially lead to large stresses and adhesion effects near the tip, causing possible membrane fracture.[15] However, a non-contact tool for the estimation of the elastic properties of 2D-materials, such as that presented in this work, can avoid these problems.

In principle, the contact between the sharp tip of AFM cantilever with the membrane could be avoided if a non-contact load (e.g., electrostatic load) is employed to induce the deflection in the suspended graphene membrane. In this regard, the static load-deflection curves of an electrostatically loaded graphene membrane have been utilized to extract its Young's modulus.[12,16] In this method, the pressure is distributed over the surface, and hence, the membrane is not in contact with a sharp tip applying non-uniform stress. Another non-contact method for extracting the mechanical properties of graphene membrane is an identification based on nonlinear resonances of the system.[17] Generally, nano-scaled resonators easily reach the nonlinear vibration regime.[18–20] In particular, for graphene, Duffing-type nonlinear responses have been regularly observed.[6,8,21] Moreover, in electrostatically actuated nano-resonators, the electrostatic load is also nonlinearly dependent on the deflection.[22] These sources of nonlinearities, which in practice emerge as hardening or softening effects in the frequency response of the system, are potentially beneficial for identification of the stiffness. In this regard, in a recent study, we have introduced a method for determining the effective Young's modulus of 2D-materials by fitting the forced nonlinear Duffing response of *large amplitude vibrations* to experimental data.[17]

In the present paper, an alternative approach for characterization of suspended graphene membranes is proposed which is based on their voltage dependent resonance frequencies. In this approach, *low amplitude vibrations* are employed for material characterization. The natural frequency of an unloaded stretched graphene membrane is a function of its pretension only.[23] However, when the membrane is subjected to a DC electrostatic load, it will deform, and this deformation, being a function of the Young's modulus, induces geometrical stiffness in the membrane that consequently leads to a shift in the resonance frequency. Hence, the resonance

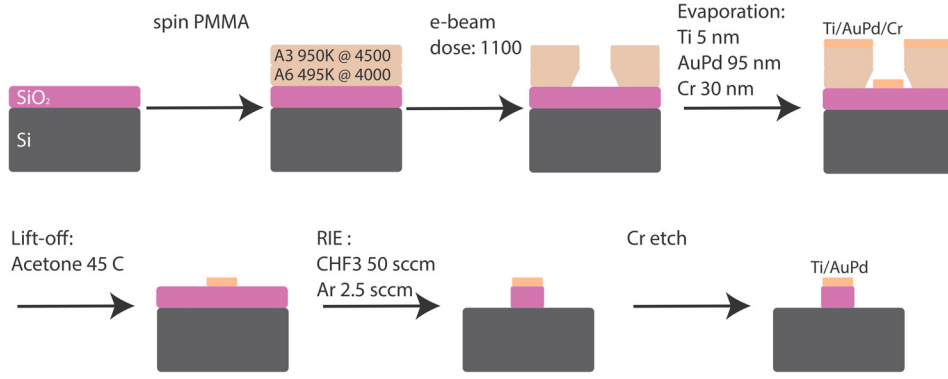a)Electronic mail: F.Alijani@tudelft.nl

FIG. 1. The schematic of the fabrication process of the electrical contacts, circular cavities, and bonding pads.

frequency of the membrane around its deformed configuration will be a function of both Young's modulus and DC voltage. By tracking the change in the resonance frequency as a function of DC voltage, one can obtain the Young's modulus.

For this purpose, the vibrations of a circular graphene resonator, electrostatically actuated around its first resonance, are studied both experimentally and theoretically. First, in order to unveil the dynamic characteristics of a graphene resonator, we perform a series of measurements on a graphene membrane subjected to simultaneous DC and AC electrostatic loads. Based on these experiments, the stretching of the graphene resonator due to high DC voltage and the shift in the resonance frequency are investigated.

Next, the vibration of graphene is modeled using an equivalent continuous membrane. The numerical model is based on a Lagrangian approach. In the model, both the nonlinear stretching of the membrane and the non-uniformity of electrostatic load due to deflection of the membrane are incorporated. To the best of the authors' knowledge, despite earlier experimental and theoretical studies on the dynamics of electrostatically actuated graphene resonators,[2,17,24,25] there is no model which accounts for in-plane degrees of freedom, geometric and electrostatic nonlinearity in a nanodrum, and yet verified with experiments.

Finally, the equivalent elastic modulus is determined by fitting the theoretically calculated shift in the resonance frequency due to DC voltage to the experimental results. In this way, (i) the Young modulus is obtained in a non-contact manner, (ii) only the resonance frequency of the system is traced, and (iii) the inaccuracy in the calibration of the amplitude around a deformed configuration will be non-influential. The validity of the proposed method is evaluated by comparing the numerical results with the experiments with high amplitude vibrations.

II. EXPERIMENTS AND DEVICE FABRICATION

To create a platform for the electrostatic 2D-nanoresonator, we start with a silicon wafer with a 285 nm thick layer of thermal silicon dioxide (SiO_2). The schematic of the fabrication process is shown in Fig. 1. Electrical contacts, circular cavities, and bonding pads are patterned on the wafer using e-beam lithography. The electrical contacts consist of a layer of Ti/AuPd, which is physically deposited (via evaporation) providing contact to the graphene membrane, together with a Cr layer, which is used as a hard mask for the

subsequent etching step (RIE). After etching, the Cr layer is removed using a wet etchant, resulting in cavities with a final depth of $d = 385$ nm and a radius of $R = 2.5\ \mu m$.

Next, flakes of graphene are exfoliated from natural crystals and are transferred on the top of the cavities using a dry transfer method.[26] The thickness of the graphene flakes is determined by AFM measurement and is equal to $h = 5$ nm, which is approximately equivalent to 15 layers of graphene. The sample is then mounted to a vacuum chamber. The schematics of the sample and the measurement set-up are illustrated in Fig. 2(a).

In order to actuate the membrane, a combination of AC and DC voltage is applied to the bonding pads using a biastee (BT), and the silicon substrate is grounded. The drum's motion is probed by a helium-neon laser. The intensity variations caused by the interfering reflections from the moving membrane and the fixed silicon substrate underneath are detected by a Newport 1801 photodiode[8] (with a responsivity
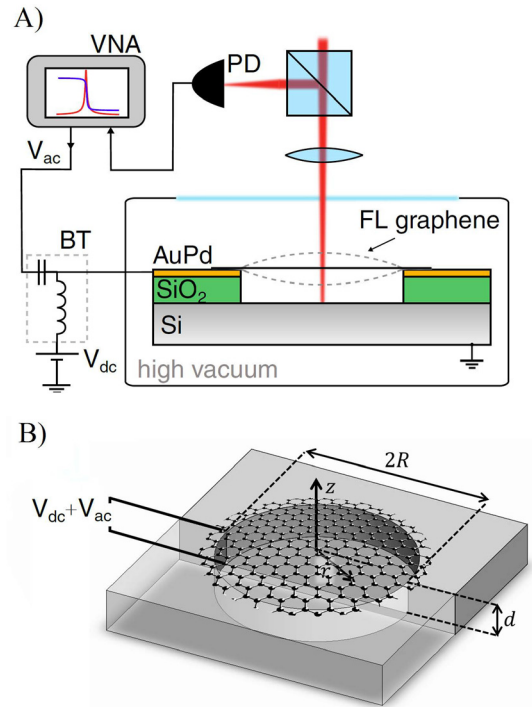

FIG. 2. Schematics of (a) device description and measurement set-up with an interferometric laser set-up to read out the motion of the membrane, and (b) the circular multilayer graphene membrane suspended above a grounded silicon substrate.

of 0.35 A/W). The detection is done in a homodyne scheme, using a Vector Network Analyser (VNA) that outputs the AC voltage in a combination with a DC voltage source. All measurements were performed using a low laser power (<1 mW) to reduce heating effects that would influence the mechanical properties of the drum.

To relate the measured amplitude to the actual motion of the membrane, a calibration measurement of the drum's Brownian motion is performed.[6] Therefore, the calibration is the most accurate around the un-deformed configuration (i.e., at small voltages). The absolute amount of static deflection of the graphene membrane when subjected to a DC voltage can be measured with the same principle. However, due to high noise floor at low frequencies, the obtained static deflection is not very accurate.

III. THEORETICAL FORMULATION

In this section, we propose a model for the harmonic response of the electrostatically actuated membrane, at its first resonance. Since the scaling effect on the dynamics of graphene membranes appears at much smaller membrane radii, we use classical continuum to obtain our model.[27] Moreover, the bending energy of the graphene membrane is orders of magnitude smaller than the energy from in-plane strain.[11] Hence, the graphene can be modeled as a membrane, without bending stiffness. This membrane is assumed to be isotropic and homogeneous.[21]

The radius of the membrane is R and its thickness is h. The Young's modulus, Poisson ratio, and the mass density of the membrane are E, ν, and μ, respectively. The membrane is suspended over a grounded electrode, and the initial gap between the two electrodes is d. The schematic model of this system is shown in Fig. 2(b). An electric potential V consisting of a DC bias voltage (V_{DC}) and an alternating AC voltage (V_{AC}) is applied to the membrane.

The alternating electrostatic field induces an alternating electrostatic load, which causes a dynamic motion in the membrane. Considering that the electrostatic load is symmetric, and the membrane is excited around its fundamental frequency, the non-axisymmetric modes will not be excited. In fact, even if the non-axisymmetric modes are accidentally excited, they will decay with time due to the presence of damping.[28] For the axisymmetric modes, the only relevant displacement components are the radial (u) and transverse (w) components. We use a reduced-order model and a Lagrangian approach to obtain the equations of motion for such a system. In this approach, the displacement components are approximated by a superposition of a finite number of suitably chosen basis functions

$$w(\rho, t) = \sum_{i=1}^{N} q_i(t) d\Phi_i(\rho), \qquad (1a)$$

$$u(\rho, t) = \xi_0 R\rho + \sum_{i=1}^{n} q_{i+N}(t) R\Psi_i(\rho), \qquad (1b)$$

where $\rho = r/R$ is the normalized radial coordinate, and $q_i(t)$ are dimensionless generalized coordinates. The parameter ξ_0

models the initial strain due to the pretension N_0 in the membrane

$$\xi_0 = \frac{N_0(1 - \nu)}{Eh}. \qquad (2)$$

The functions $\Phi_i(\rho)$ and $\Psi_i(\rho)$ are basis-functions satisfying the boundary conditions. Here, axisymmetric linear mode shapes of a clamped membrane are utilized as the transverse basis-functions

$$\Phi_i(\rho) = J_m(\lambda_{mi}\rho), \qquad i = 1...N, \qquad (3)$$

where J_m is the mth order Bessel function of the first kind. In fact, m is the number of nodal circles, and λ_{mi} is the ith positive root of J_m. Figure 3 shows the first three associated mode-shapes. The in-plane basis-functions (Ψ_i), satisfying continuity and symmetry at $\rho = 0$, are

$$\Psi_i(\rho) = \rho^i(1 - \rho), \quad i = 1...n. \qquad (4)$$

Next, the strain components of the membrane are calculated as follows:

$$\varepsilon_r = \frac{1}{R}\frac{\partial u}{\partial \rho} + \frac{1}{2R^2}\left(\frac{\partial w}{\partial \rho}\right)^2, \qquad (5a)$$

$$\varepsilon_\theta = \frac{1}{R}\frac{u}{\rho}, \qquad (5b)$$

$$\varepsilon_{r\theta} = 0. \qquad (5c)$$

The total potential energy of the system consists of two terms: the electrostatic potential (U_e) and the potential associated with elastic deformation due to the stretching (U_s) of the membrane

$$U = U_s + U_e. \qquad (6)$$

The elastic potential (U_s) can be approximated by[29]

$$U_s = \frac{EhR^2}{2(1 - \nu^2)} \int_0^{2\pi} \int_0^1 \left(\varepsilon_r^2 + \varepsilon_\theta^2 + 2\nu\varepsilon_r\varepsilon_\theta + \frac{1 - \nu}{2}\varepsilon_{r\theta}^2\right)\rho\,d\rho\,d\theta, \qquad (7)$$

and the electrostatic potential, assuming parallel-plate capacitor theory, can be evaluated as[30]

$$U_e = -(1 - \alpha)\frac{1}{2}\epsilon V^2 R^2 \int_0^{2\pi} \int_0^1 \frac{\rho}{d + w}\,d\rho\,d\theta. \qquad (8)$$

The constant ϵ is the electric permittivity of the dielectric between the electrodes and V is the applied voltage. Moreover, α provides a global correction for the electrostatic load and is

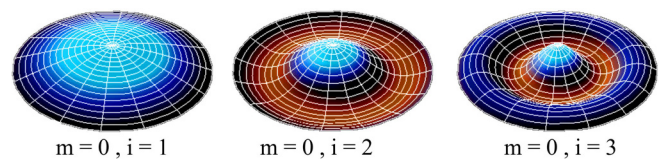m = 0 , i = 1   m = 0 , i = 2   m = 0 , i = 3

FIG. 3. The first three axi-symmetric mode-shapes of a membrane with clamped contour, indexed by i and m.

the ratio between the actual load applied to the membrane and that of the ideal parallel plate capacitor. This factor is dominated by the fringing field effects which in our set-up are mainly due to the electrostatic field between the silicon substrate and the side edge of Ti/AuPd layer in the cavity. However, it can also account for the nano-scale effects that can change the capacitance of the system.[31,32] This factor can vary for different set-ups between 0 and 1, depending on the configuration of the capacitor, and hence, it should be calibrated for each experimental set-up, separately. In this study, we have obtained this parameter using the experimental results in the low amplitude vibrations. For simplicity, we assume that α does not depend on the deflection of the membrane.

Notice that in formulating the electrostatic potential (U_e), the local distance between the electrodes ($d + w$) is used, where w can be expressed as in (1a). When the membrane is excited around the first resonance, the dominant shape of the motion can be mimicked with the first mode shape, and therefore, the effect of higher modes in the electrostatic load can be neglected. Hence, the electrostatic potential is simplified to

$$U_e = -(1 - \alpha)\pi\epsilon V^2 R^2 \int_0^1 \frac{\rho \, \mathrm{d}\rho}{d + dq_1(t)\Phi_1(\rho)}. \quad (9)$$

To calculate the energy associated with the electrostatic potential, the function inside the integral in Eq. (9) is written as a Taylor series expansion in terms of $q_1(t)$ around the undeformed configuration ($q_1(t) = 0$). The electric potential $V(t)$ in Eqs. (8) and (9) consists of a DC bias voltage V_{DC}, and an alternating AC voltage with a root-mean-square (RMS) of V_{AC} and excitation frequency Ω; thus

$$V = V_{DC} + \sqrt{2}V_{AC}\sin(\Omega t). \quad (10)$$

Next, the kinetic energy of the system can be expressed as

$$T = \pi\mu R^2 h \int_0^1 (\dot{w}^2 + \dot{u}^2)\rho \, \mathrm{d}\rho, \quad (11)$$

where the overdot indicates differentiation with respect to time. Employing the relations given in Eqs. (1a)–(11), the Lagrangian of the system $L = T - U$ can be expressed as a nonlinear function of generalized coordinates $L(q_i, \dot{q}_i, t)$. Then, the Lagrange equations can be employed to obtain the equations of motion

$$\frac{\partial L}{\partial q_i} = \frac{\mathrm{d}}{\mathrm{d}t}\left(\frac{\partial L}{\partial \dot{q}_i}\right). \quad (12)$$

As a result, $N + n$ nonlinear equations governing the motion of the nano-membrane will be obtained. It should be noted here that, in practice, the system will possess some kind of energy dissipation or damping. Assuming modal damping, Eq. (12) gives a system of nonlinear ordinary differential equations,

$$\bar{\bar{\mathbf{M}}}\ddot{\mathbf{q}} + \bar{\bar{\mathbf{C}}}\dot{\mathbf{q}} + \left[\bar{\bar{\mathbf{K}}}(N_0) + \bar{\bar{\mathbf{N}}}_2(\mathbf{q}) + \bar{\bar{\mathbf{N}}}_3(\mathbf{q}, \mathbf{q})\right]\mathbf{q} = \bar{\mathbf{F}}(\mathbf{q}), \quad (13)$$

where $\bar{\bar{\mathbf{M}}}$ is the mass matrix, and $\bar{\bar{\mathbf{C}}}$ is the damping matrix which is added to the equations of motion to describe

dissipation. $\bar{\bar{\mathbf{K}}}$ is the stiffness matrix and is a function of the pretension,[23] and it determines, together with the mass of the membrane, the natural frequency of the unloaded configuration. $\bar{\bar{\mathbf{N}}}_2$ and $\bar{\bar{\mathbf{N}}}_3$ are matrices which are linear and quadratic functions of the generalized coordinates, respectively, and when multiplied by $\mathbf{q}$, they cause quadratic and cubic (Duffing) nonlinearities in the equations. These matrices are functions of the Young's modulus of the membrane, as well, and are a consequence of adopting nonlinear (von Kármán) membrane theory. Moreover, $\bar{\mathbf{F}}$ is the nonlinear generalized electrostatic force vector whose components are expressed as

$$\begin{aligned} F_i(t) &= -\frac{1}{2}\epsilon V^2(1 - \alpha)\frac{\pi R^2}{d^2}F(q_1) & i = 1, \\ F_i(t) &= 0 & i > 1. \end{aligned} \quad (14)$$

The function $F(q_1)$ is a polynomial which captures the nonlinearity of the electrostatic load and its nonuniform distribution on the deflected membrane. The accuracy of the function $F(q_1)$ depends on the truncation of the Taylor series employed for approximating the integral in Eq. (9). Figure 4 shows different approximations of function F and it indicates that by using a Taylor series of fifth order, good convergence will be achieved.

In order to perform numerical integration, Eq. (13) is multiplied by the inverse of the mass matrix and then recast into first-order ordinary differential equations by introducing the dummy vector $\mathbf{y}$, as follows:

$$\dot{\mathbf{q}} = \mathbf{y},$$

$$\dot{\mathbf{y}} = -\bar{\bar{\mathbf{M}}}^{-1}\bar{\bar{\mathbf{C}}}y - \bar{\bar{\mathbf{M}}}^{-1}[\bar{\bar{\mathbf{K}}}(N_0) + \bar{\bar{\mathbf{N}}}_2(\mathbf{q}) + \bar{\bar{\mathbf{N}}}_3(\mathbf{q}, \mathbf{q})]\mathbf{q}$$

$$+ \bar{\bar{\mathbf{M}}}^{-1}\bar{\mathbf{F}}(\mathbf{t}), \quad (15)$$

where $\bar{\bar{\mathbf{M}}}^{-1}\bar{\bar{\mathbf{C}}}$ is the dissipation term, which is assumed to be diagonal based on the assumption of modal damping, and is expressed as

$$\begin{aligned} \left[\bar{\bar{\mathbf{M}}}^{-1}\bar{\bar{\mathbf{C}}}\right]_{\mathbf{ij}} &= \mathbf{2}\omega_{\mathbf{i}}\xi_{\mathbf{i}} & i = j \\ \left[\bar{\bar{\mathbf{M}}}^{-1}\bar{\bar{\mathbf{C}}}\right]_{\mathbf{ij}} &= \mathbf{0} & i \neq j. \end{aligned} \quad (16)$$
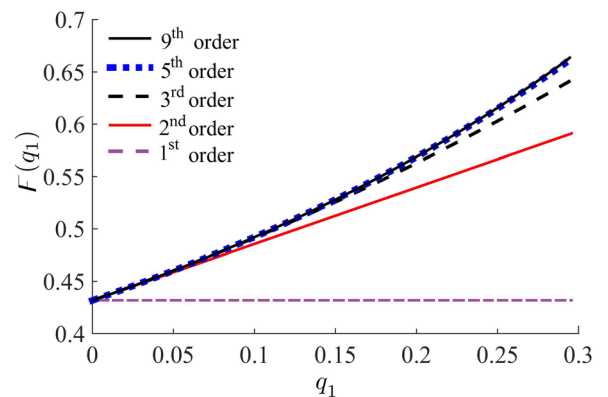

FIG. 4. The nonlinear electrostatic potential is approximated by a polynomial function with different orders. The approximated electrostatic load converges when a 5th order polynomial is employed.

In Eq. (16), ω_i are the natural frequencies obtained from the characteristic equation of the system (i.e., $\det[\omega_i^2 \bar{\bar{\mathbf{M}}} - \bar{\bar{\mathbf{K}}}] = 0$), and ξ_i are the corresponding modal damping ratios of each generalized coordinate.

To study the periodic solutions and the frequency response of the system, a pseudo arc-length continuation and collocation scheme have been used.[33] In particular, a continuation is carried out in three steps: (i) The continuation starts at a trivial steady state solution, zero AC and DC voltages, with a small excitation frequency much below the resonance. (ii) In the second step, the load parameter V_{DC} is chosen as the continuation parameter. Once the desired parameter value is reached, V_{AC} is introduced as the continuation parameter, until the desired value is reached. Unstable solution branches are avoided in this step. (iii) The rest of the analysis is performed by considering the excitation frequency Ω as the continuation parameter. In this step, the continuation is performed around the first resonance of the system and the stability of the solution branches is determined using the Floquet theory.[34]

IV. EXTRACTING THE EQUIVALENT YOUNG'S MODULUS FROM THE RESONANCE FREQUENCY

In this section, we demonstrate the concept of extracting Young's modulus from the fundamental frequency of a pretensioned membrane subjected to a high DC voltage and low AC. For this reason, we obtain the static deflection of the membrane due to the applied DC voltage and linearize the equation of motion [i.e., Eq. (13)] around this configuration. While solving Eq. (13), the force vector can be split into static and dynamic components

$$\bar{\mathbf{F}} = \bar{\mathbf{F}}_{\mathbf{s}} + \bar{\mathbf{F}}_{\mathbf{d}}, \tag{17}$$

where if $V_{AC} \ll V_{DC}$, the dynamic force is much smaller than the static force. Similarly, the solution can be split into two parts,

$$\mathbf{q} = \mathbf{q}_{\mathbf{s}} + \mathbf{q}_{\mathbf{d}}, \tag{18}$$

where $\mathbf{q}_{\mathbf{s}}$ and $\mathbf{q}_{\mathbf{d}}$ are the static and dynamic solutions, respectively. The static deflection, $\mathbf{q}_{\mathbf{s}}$, can be estimated by letting $\bar{\mathbf{F}}_{\mathbf{d}} = 0$ and $\ddot{\mathbf{q}} = \dot{\mathbf{q}} = 0$, leading to

$$\left[\bar{\bar{\mathbf{K}}}(N_0) + \bar{\bar{\mathbf{N}}}_2(\mathbf{q}_{\mathbf{s}}) + \bar{\bar{\mathbf{N}}}_3(\mathbf{q}_{\mathbf{s}}, \mathbf{q}_{\mathbf{s}}) \right] \mathbf{q}_{\mathbf{s}} = \bar{\mathbf{F}}_{\mathbf{s}}. \tag{19}$$

The solution of this algebraic set of equations provides $\mathbf{q}_{\mathbf{s}}$ as a function of DC voltage and elastic modulus. A relatively small AC voltage will lead to a *linear* vibration around this static configuration. The dynamic analysis in such a configuration shall be performed for determining the final state of vibration by adding an incremental dynamic solution $\mathbf{q}_{\mathbf{d}}$ to the static solution $\mathbf{q}_{\mathbf{s}}$. By subtracting Eq. (19) from (13), and neglecting the higher order terms in $\mathbf{q}_{\mathbf{d}}$, the following system of *linear* ordinary differential equations is obtained:

$$\bar{\bar{\mathbf{M}}}\ddot{\mathbf{q}}_{\mathbf{d}} + \bar{\bar{C}}\dot{\mathbf{q}}_{\mathbf{d}} + \underbrace{\left[\bar{\bar{\mathbf{K}}}(N_0) + \bar{\bar{\mathbf{N}}}_2'(\mathbf{q}_{\mathbf{s}}) + \bar{\bar{\mathbf{N}}}_3'(\mathbf{q}_{\mathbf{s}}, \mathbf{q}_{\mathbf{s}}) \right]}_{\bar{\bar{\mathbf{K}}}'(\mathbf{q}_{\mathbf{s}}, E, N_0)} \mathbf{q}_{\mathbf{d}} = \bar{\mathbf{F}}_{\mathbf{d}}. \tag{20}$$

In this equation, $\bar{\bar{\mathbf{N}}}_2'$ and $\bar{\bar{\mathbf{N}}}_3'$ are associated with nonlinearities in $\mathbf{q}_{\mathbf{s}}$. Equation (20) describes the linear vibrations of the membrane subjected to a relatively small AC voltage around a static configuration ($\mathbf{q}_{\mathbf{s}}$). The resonance frequencies (ω') can be obtained from the characteristic equation of this new dynamic system as a function of the static deflection $\mathbf{q}_{\mathbf{s}}$, pretension N_0, and the Young's modulus

$$|\omega'^2 \bar{\bar{\mathbf{M}}} - \bar{\bar{\mathbf{K}}}'(\mathbf{q}_{\mathbf{s}}, E, N_0)| = 0, \tag{21}$$

where the static deflection $\mathbf{q}_{\mathbf{s}}$ has been obtained as a function of DC voltage from (19). An example of the application of Eq. (21), for the case in which one transverse and two in-plane degrees-of-freedom are retained, is given in A. With Eq. (21), the experimental value of ω' can be used to determine the equivalent Young's modulus E, if N_0 and $\mathbf{q}_{\mathbf{s}}$ are known.

In order to extract the equivalent Young's modulus from the experimental data, four fundamental steps are taken:

(I)   The pretension (N_0) is determined by matching the fundamental frequency of the system in the unloaded configuration ($V_{DC} = 0$) to that of experimental results (ω_0)

$$|\omega_0^2 \bar{\bar{\mathbf{M}}} - \bar{\bar{\mathbf{K}}}(N_0)| = 0. \tag{22}$$

(II)   The damping ratio of the first resonance frequency (ξ_1) is obtained by fitting the low amplitude response curves.[35]

(III) The force correction factor (α) is determined by matching the numerical amplitude of the system (A_0) in low-amplitude vibrations, to the calibrated experimental data.[6] For small DC and AC voltages, one can simply ignore the geometric and electrostatic nonlinearity, and assume harmonic oscillations. Therefore,[36]

$$A_0 = (1 - \alpha)F(0)\frac{\epsilon \pi R^2}{d^2}\frac{V_{AC}V_{DC}}{2\xi_1 \bar{\bar{\mathbf{K}}}_{11}}. \tag{23}$$

(IV)   Using the obtained pretension and force correction factor, the fundamental frequency (ω') of the system is obtained numerically for a range of nonzero DC voltages. The resonance frequency can be obtained from the approximation in Eq. (21) or from the results of full model as explained in Sec. III, which will capture the electrostatic softening as well. The equivalent Young's modulus of the membrane is then achieved by fitting *the voltage dependent shift in resonance frequency* (ω') to the experimental results.

V. RESULTS AND DISCUSSION

In this section, the results of the experiments and theoretical studies are reported, and the suitability of the proposed numerical model as a tool for characterization of the graphene membrane and analyzing its nonlinear vibrations is investigated.

A. Experiments

Figure 5 shows a set of experimental forced vibration responses around the fundamental frequency while varying
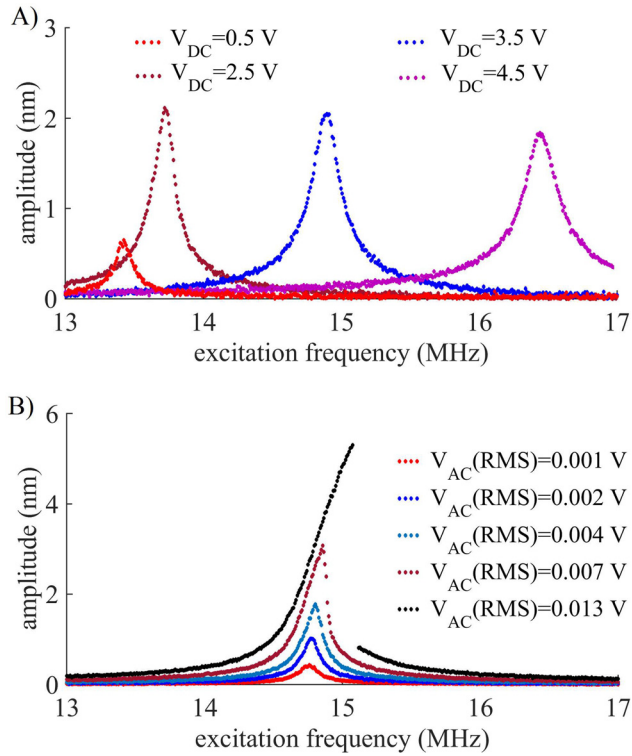
A)

B)

FIG. 5. The measured amplitude of the motion as a function of excitation frequency, (a) with a small AC voltage of $V_{AC} = 4.5$ mV, and different DC voltages, and (b) with different AC voltages and a DC voltage of $V_{DC} = 3$ V. The measurements are taken at the center of the drum.

the driving DC and AC voltages. The deflection was measured at the center of the membrane, where the fundamental mode shape presents the largest amplitude. In the first set, the AC voltage is kept fixed (with a low RMS value of 4.5 mV) and the change in the linear resonance of the system is traced by varying the DC voltage. The natural frequency (i.e., when $V_{DC} = 0$ V) was obtained to be 13.4 MHz. This frequency has been used to obtain the pretension in the membrane. The resonance frequency slightly decreases when a small DC voltage is applied to the system, e.g., at $V_{DC} = 0.5$ V, the resonance occurs at 13.36 MHz. The frequency response of the system at this configuration is used to obtain the force correction factor. When a higher DC voltage is applied, the resonance frequency increases [see Fig. 5(a)]. This change in resonance frequency is due to electrostatic (softening) and then the geometrical (hardening) nonlinearity. However, the frequency response function of the membrane remains linear.

It should be noticed that the maximum amplitude of the vibrations at the resonance varies with the applied DC voltage, as well. As a matter of fact, the maximum amplitude is defined by the stiffness of the system and the dynamic load, both of which depend on the DC voltage. This dependence causes the maximum amplitude to increase with the DC voltage due to a larger dynamic load, and later decrease due to higher geometrical stiffness induced in the membrane and higher damping.

Figure 5(b) shows the experimental frequency response curves obtained by keeping the DC voltage constant at 3 V and varying the AC voltage from 0.001 V to 0.013 V. As can

be observed, at AC voltages above 0.004 V, the system exhibits nonlinear hardening behavior. At $V_{AC} = 0.013$ V, the system shows a clear instability and therefore a jump right after the resonance.

B. Validation of the numerical model

The procedure outlined in Sec. III has been applied to a membrane with the following properties: $\nu = 0.165$, $\mu = 2.2388$ g/cm^3, $h = 5$ nm, $R = 2.5\,\mu$m and $d = 385$ nm. Moreover, a relatively low damping ratio ($\xi_i = 0.002$) is considered in the following numerical results. In the validation of the numerical model, the effect of force correction factor is ignored ($\alpha = 0$).

In the Lagrangian approach, basis functions are employed to approximate the exact solution of the problem, and therefore, a convergence analysis is required to confirm the accuracy of the described deflection. In order to find the minimum number of degrees of freedoms required to accurately model the motion of the membrane (N and n), two convergence analyses (static and dynamic) have been performed. In both analyses, the Young's modulus of pristine graphene [i.e., $E = 1150$ GPa (Ref. 37)] is considered. The static deflection of the membrane as a function of the applied DC voltage, when considering different numbers of degrees of freedom, is shown in Fig. 6. The DC voltage is varied from 0 to 10 V in the absence of V_{AC}. As can be observed, the static solution converges when 5 degrees of freedom are used in the numerical model (with two transverse and three in-plane basis functions).

In the dynamic convergence analysis, the membrane is assumed to be subjected to a DC voltage of $V_{DC} = 1$ V and a high AC voltage with the root-mean-square (RMS) of 0.025 V. The steady state solution of the membrane is calculated in a frequency range around the first resonance. Figure 7 shows the nonlinear frequency responses of the membrane when considering different numbers of degrees of freedom. In particular, Fig. 7(a) shows the effect of additional in-plane basis functions on the nonlinear dynamic response and Fig. 7(b) shows the effect of additional transverse basis functions. It can be observed that the dynamic solution also converges with five degrees of freedom (with two transverse and three in-plane mode-shapes). Therefore, all the following numerical results are obtained by using a model including these five degrees of
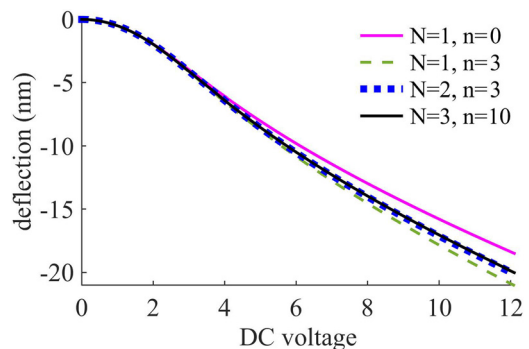

FIG. 6. Deflection of the membrane when $E = 1150$ GPa, $N_0 = 0.085$ N/m, V_{AC} (RMS) = 0 V, calculated with different numbers of degrees of freedom. The solution converges at 5 degrees of freedom (N = 2 and n = 3).
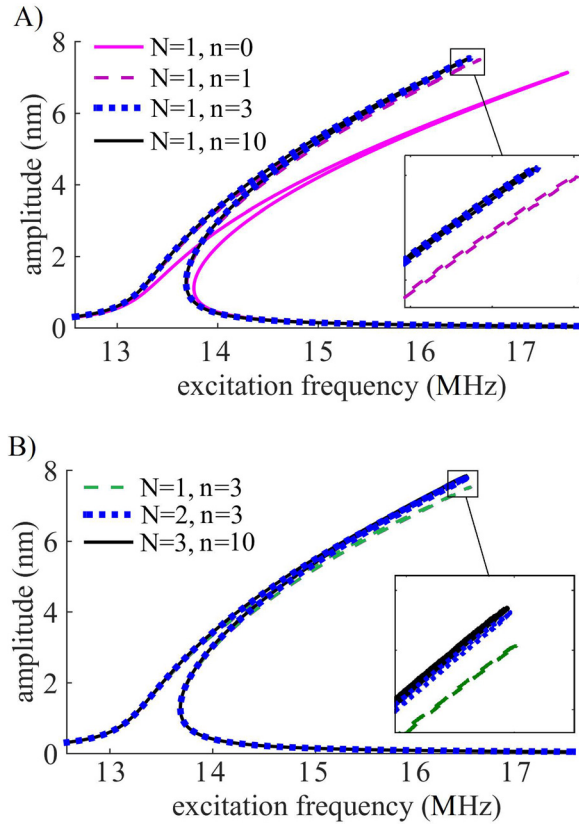
FIG. 7. Root-mean-square amplitude of the membrane when $E = 1150\,GPa$, $N_0 = 0.085\,N/m$, $\xi = 0.002$, V_{AC} (*RMS*) $= 0.02\,V$, and $V_{DC} = 1\,V$, numerically calculated with (a) different numbers of in-plane degrees of freedom and (b) transverse degrees of freedom. The solution around the first resonance converges with 5 degrees of freedom ($N = 2$ and $n = 3$).

freedom. In calculating the electrostatic potential in Eq. (9), the contribution of higher modes was neglected assuming $q_1 \gg q_i$ for $i > 1$. In order to check the validity of this assumption, the time response and phase portrait of the first two transverse modes of the system, right before the nonlinear resonance (15.6 MHz), are shown in Fig. 8. The graphs in this figure are obtained using the same parameter values as in Figs. 6 and 7. As can be noticed, the maximum amplitude and time derivative of the second mode are an order of magnitude smaller than the amplitude and time derivative of the first mode.

Finally, to verify the efficiency of the proposed model, an eigen-frequency analysis has been performed for a 3D finite element model built in COMSOL Multiphysics and compared with the present model. In the COMSOL model, the membrane is modeled with the same characteristics as in the convergence analysis and is discretized with fine mesh consisting of shell elements. The surface of the membrane is loaded with a nonlinear electrostatic load similar to the analytical formulation (i.e., $\epsilon \frac{-V_{dc}^2}{2(d+w)^2}$), where V_{dc} is a parameter representing the DC voltage. The eigen-frequency of the deflected system for a range of V_{dc} is obtained while incorporating the geometrical stiffness.

Figure 9 shows the obtained linear resonance frequency, as a function of the applied voltage. For comparison, the graphs obtained by the proposed model, finite element
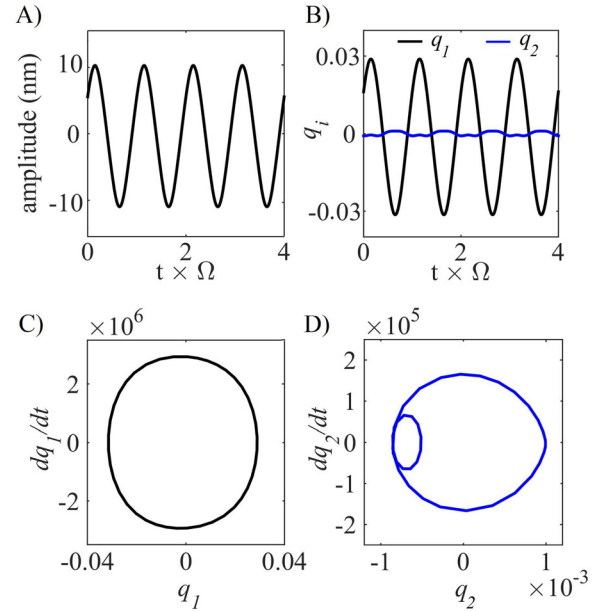

FIG. 8. Time response of (a) the deflection at the center of the membrane and (b) the first two mode shapes, and a two-dimensional projection of the phase portrait of (c) first, and (d) second modes, slightly before the resonance ($\Omega = 16.5\,GHz$), using $E = 1150\,GPa$, $N_0 = 0.085\,N/m$, $\xi = 0.002$, V_{AC} (*RMS*) $= 0.02\,V$, and $V_{DC} = 1\,V$.

model, and also the approximate model proposed by Ref. 25 are shown. As can be observed, the proposed model is perfectly matching the results of the FEM solution, while the single degree of freedom model of Ref. 25 diverges from these two solutions. This figure demonstrates the accuracy of the proposed method in capturing the effect of DC voltage on the resonance frequency of the membrane.

C. Extracting the equivalent Young's modulus

In order to find the accurate equivalent Young's modulus, we compare the experimentally observed change in the resonance frequency with the numerical results. Based on the experimental results, a pretension of $N_0 = 0.0857\,N/m$ matches the natural frequency at zero DC voltage to the experiments and a force correction factor of $1 - \alpha = 0.75$ matches the maximum amplitude of low-amplitude vibrations. Moreover, a range of damping ratios ($\xi_1 = 0.0038$–0.0040), monotonically
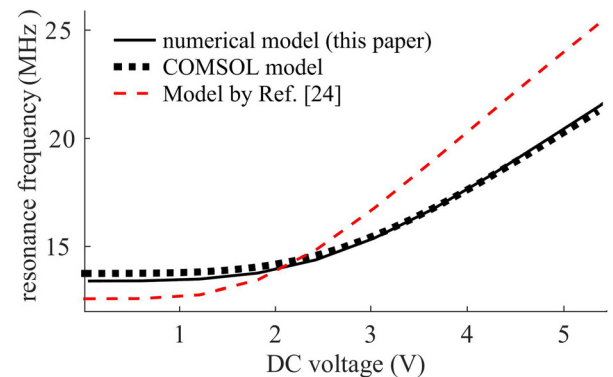

FIG. 9. The numerical resonance frequency of the excited membrane as a function of the applied DC voltage obtained by different models, using $E = 1150\,GPa$, $N_0 = 0.085\,N/m$, $\xi = 0.002$, and V_{AC} (*RMS*) $= 4.5\,mV$.
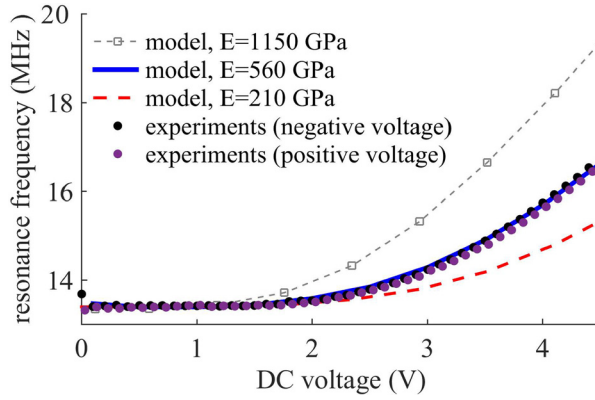
FIG. 10. The measured resonance frequency of the excited membrane as a function of the applied DC voltage, while $V_{AC}(RMS) = 4.5$ mV, and the corresponding curve obtained numerically using $E = 210$ GPa, $E = 560$ GPa, and $E = 1150$ GPa when $N_0 = 0.0857$ N/m and $\alpha = 0.25$.

increasing with DC voltage, is obtained from the experiments. In the model, we have employed the same damping ratio for the other modes of vibrations.

Figure 10 shows the obtained resonance frequency as a function of the applied DC voltage. For illustrating the effect of employing different elastic moduli, the numerical results for $E = 210$ GPa, $E = 560$ GPa, and that of pristine graphene [$E = 1150$ GPa (Ref. 37)], are shown. It can be observed that the numerical results for $E = 560$ GPa are in good agreement with the experimental observations. In other words, the proposed model with this Young's modulus is able to capture the nonlinear hardening of the electrostatically actuated graphene membrane.

In order to verify the accuracy of the obtained Young's modulus, the trend of nonlinearity by varying the AC voltage is compared with the associated experimental data.[17] Figure 11 presents the amplitude of vibration at the center of the graphene membrane for a constant DC voltage (3 V) and different AC voltages, as expressed in Eq. (13). As can be observed, a very good agreement is found between the experimental and numerical results for different applied dynamic loads. The numerical results in Fig. 11 show that there are two bifurcation points associated with jump up and down in the vibration amplitude. However, the jump up bifurcation point is not evident from the experimental data, because the experiments were performed by forward frequency sweeps only.
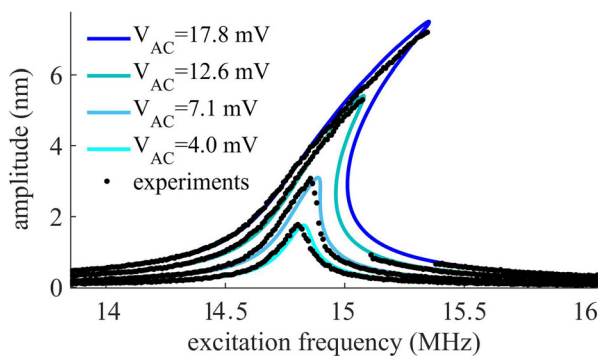

FIG. 11. Measured traces (black scatter plot) and the corresponding curves obtained numerically (solid curves) using $E = 560$ GPa, and a modal damping ratio of $\xi = 0.004$ while $V_{DC} = 3$ V.
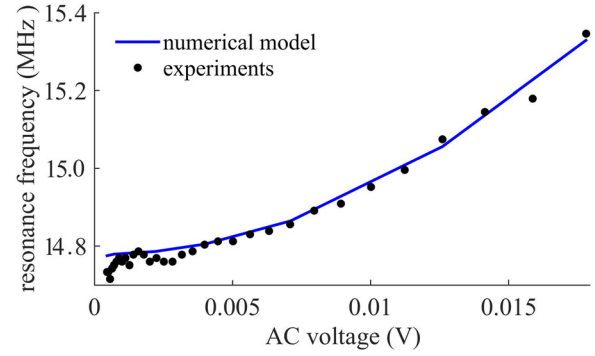

FIG. 12. The measured resonance frequency of the excited membrane as a function of the applied AC voltage, while $V_{DC} = 3$ V, and the corresponding curve obtained analytically using $E = 560$ GPa.

It is worth mentioning that the nonlinear hardening observed in the frequency response of the excited membrane is induced by the quadratic and cubic terms in Eq. (13), which appear in $\bar{\bar{\mathbf{N}}}_2$, $\bar{\bar{\mathbf{N}}}_3$, and $\bar{\bar{\mathbf{F}}}(\mathbf{q})$. Therefore, not only the Young's modulus, but also the applied DC voltage has an influence on the nonlinearity, which if neglected, might be mistaken with Duffing type nonlinearity.

The nonlinear resonance frequency of the system (the peaks in Fig. 11) varies with the applied AC voltage. This change is illustrated more specifically in Fig. 12. Due to the presence of the static DC voltage, the resonance frequency of the system has a shift with respect to the free-vibration fundamental frequency (13.6 MHz), and by increasing the
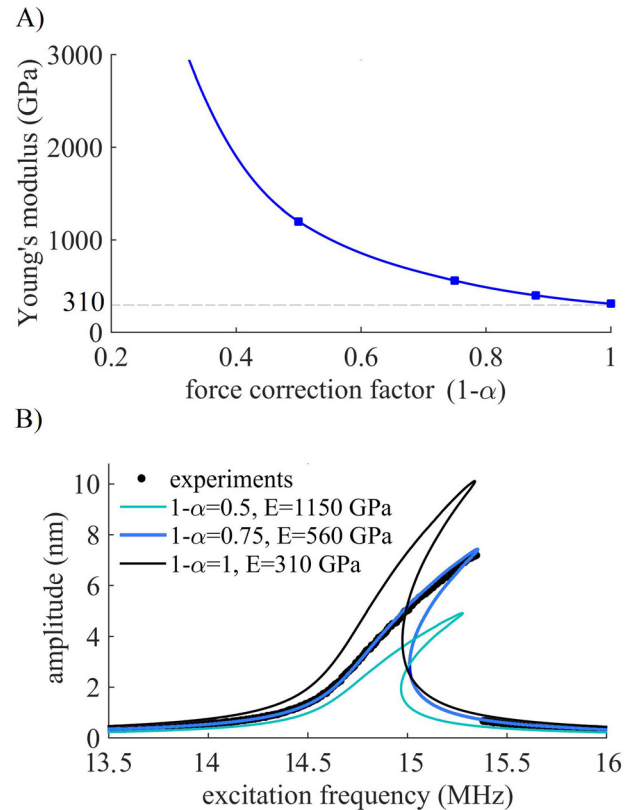

FIG. 13. (a) The matching Young's modulus as a function of the force correction factor $(1 - \alpha)$, and (b) measured traces (black scatter plot) and the corresponding curves obtained numerically with different force correction factors, while $V_{DC} = 3$ V and $V_{AC} = 17.8$ mV.

dynamic load (AC voltage), the system exhibits a nonlinear hardening and the resonance frequency increases further. The overall trend of the hardening of the system obtained numerically with $E = 560$ GPa is in good agreement with the experiments, which confirms the accuracy of the obtained Young's modulus.

Finally, we shall stress that the correct evaluation of the force correction factor employed in Eq. (8) is a crucial aspect in characterization of the Young's modulus. Figure 13(a) shows the obtained Young's modulus which matches the voltage dependent frequency shift as a function of this factor. As can be observed, an inaccurate estimation of this factor can result in incorrect characterization of the Young's modulus. If this correction factor is neglected, the corresponding elastic modulus will be obtained as 310 GPa. As shown in Fig. 13(b), if an inaccurate correction factor is employed to obtain the Young's modulus, the numerical results will not match the high amplitude vibrations.

VI. CONCLUSIONS

Resonance frequency tuning of an electrostatically actuated multi-layer graphene membrane with a DC voltage has been introduced as a tool for the evaluation of its equivalent Young's modulus. For this purpose, using an energy approach based on a Lagrange formulation, the equations of motion were derived and solved numerically. The proposed model extends the earlier work on electrostatically actuated graphene membranes,[25] by including not only transverse, but also radial displacements of the graphene. Moreover, based on a comparison with a detailed finite elements solution, it has been shown that the proposed model can capture the effect of DC voltage on the frequency response accurately.

In this study, experiments were performed to explore the linear and nonlinear vibrations of an electrostatically actuated graphene membrane. As a result, the shift in resonance frequency and nonlinear hardening and softening behavior, due to geometrical and electrostatic nonlinearities, have been investigated. It was shown that by comparing the model with experimental data, the pretension, the force correction factor, and the Young's modulus of the graphene can be determined. The obtained Young's modulus also closely matched the nonlinear dynamics of the membrane, providing evidence for suitability of this method for extracting the Young's modulus of the 2D-nano-resonators.

Moreover, it was found that the accurate estimation of the electrostatic load is one of the most crucial factors in this method of characterization of the Young's modulus. For a parallel plate capacitor, the fringing fields effects can be calculated theoretically. However, the fringing field, although probably the most dominant, is one out of many other factors influencing the electrostatic load.[31,32] Therefore, it is most efficient to extract this factor directly from the experimental results.

It should be mentioned that the obtained value of the Young's modulus ($E = 560$ GPa) is lower than the reported value in the literature for pristine graphene. This difference, which has been repeatedly reported in other experimental studies,[38] is hypothesized to be the result of wrinkles, ripples, or defects in the graphene. Defects such as wrinkles

and ripples,[12,14] or grained size of the polycrystalline,[38,39] may affect the elasticity of the graphene to a large extent.

The proposed method for extracting the Young's modulus is non-contact and non-destructive, and it does not require calibration of the amplitude of vibrations in high DC voltages. In addition, this method is simple to implement and is computationally efficient.

APPENDIX A: VOLTAGE DEPENDENT FUNDAMENTAL FREQUENCY OF THE GRAPHENE MEMBRANE

To simplify the equations, the in-plane inertia is neglected and the Poisson ratio is assumed as $\nu = 0.17$. Using one transverse and two in-plane degrees of freedom (N = 1 and n = 2), Eq. (13) simplifies to

$$m\ddot{q} + 2\xi\sqrt{\frac{k_1}{m}}\dot{q} + k_1 q + k_3 q^3 = -\frac{1}{2}\epsilon V^2(1-\alpha)\frac{\pi R^2}{d^2}F(q), \tag{A1}$$

where q is the transverse deflection of the nano-membrane normalized with respect to the gap size d. The other parameters are defined as

$$\begin{aligned} m &= 0.269\pi R^2 h\mu d, \\ k_1 &= \pi 1.558 dN_0, \\ k_3 &= \frac{\pi 0.913 Eh}{R^2}d^3. \end{aligned} \tag{A2}$$

Moreover, the function $F(q)$ which captures the nonlinearity of the electrostatic load and its nonuniform distribution on the deflected membrane can be expressed as

$$\begin{aligned} F(q) =& -0.6352q^5 + 0.625q^4 - 0.609q^3 \\ & + 0.584q^2 - 0.539q + 0.432. \end{aligned} \tag{A3}$$

Consequently, the static equilibrium due to a DC voltage [i.e., Eq. (19)] can be obtained by solving the following algebraic equation:

$$k_1 q_s + k_3 q_s^3 = -\frac{1}{2}\epsilon V_{DC}^2(1-\alpha)\frac{\pi R^2}{d^2}F(q). \tag{A4}$$

The linearized equation of motion at this configuration can be obtained as

$$m\ddot{q}_d + 2\xi\sqrt{\frac{k_1}{m}}\dot{q}_d + \left[k_1 + 3k_3 q_s^2\right]q_d = F_d. \tag{A5}$$

Therefore, the linear resonance frequency of graphene membrane when subjected to a DC voltage can be expressed by

$$\omega' = \sqrt{\frac{k_1 + 3k_3 q_s^2}{m}} = \sqrt{\frac{5.78 N_0}{h\mu R^2} + \frac{10.20 E d^2 q_s^2}{\mu R^4}}. \tag{A6}$$

The Young's modulus E can be extracted by matching Eq. (A6) to the experimental data. This few degrees of freedom can describe the motion of the graphene membrane in low DC voltages and if the dynamic motion around the static deflection remains linear (see Figs. 6 and 7).

[1]F. Schedin, A. Geim, S. Morozov, E. Hill, P. Blake, M. Katsnelson, and K. Novoselov, "Detection of individual gas molecules adsorbed on graphene," Nat. Mater. **6**, 652–655 (2007).

[2]C. Chen, S. Rosenblatt, K. I. Bolotin, W. Kalb, P. Kim, I. Kymissis, H. L. Stormer, T. F. Heinz, and J. Hone, "Performance of monolayer graphene nanomechanical resonators with electrical readout," Nat. Nanotechnol. **4**, 861–867 (2009).

[3]R. J. Dolleman, D. Davidovikj, S. J. Cartamil-Bueno, H. S. van der Zant, and P. G. Steeneken, "Graphene squeeze-film pressure sensors," Nano Lett. **16**, 568–571 (2016).

[4]P. Li, B. Zhang, and T. Cui, "Towards intrinsic graphene biosensor: A label-free, suspended single crystalline graphene sensor for multiplex lung cancer tumor markers detection," Biosens. Bioelectron. **72**, 168–174 (2015).

[5]D. Garcia-Sanchez, A. M. van der Zande, A. S. Paulo, B. Lassagne, P. L. McEuen, and A. Bachtold, "Imaging mechanical vibrations in suspended graphene sheets," Nano Lett. **8**, 1399–1403 (2008).

[6]D. Davidovikj, J. J. Slim, S. J. Cartamil-Bueno, H. S. van der Zant, P. G. Steeneken, and W. J. Venstra, "Visualizing the motion of graphene nanodrums," Nano Lett. **16**, 2768–2773 (2016).

[7]S. Lee, C. Chen, V. V. Deshpande, G.-H. Lee, I. Lee, M. Lekas, A. Gondarenko, Y.-J. Yu, K. Shepard, and P. Kim, "Su-8 clamped CVD graphene drum resonators," preprint arXiv:1612.04279 (2016).

[8]J. S. Bunch, A. M. Van Der Zande, S. S. Verbridge, I. W. Frank, D. M. Tanenbaum, J. M. Parpia, H. G. Craighead, and P. L. McEuen, "Electromechanical resonators from graphene sheets," Science **315**, 490–493 (2007).

[9]H. Tian, Y. Shu, X.-F. Wang, M. A. Mohammad, Z. Bie, Q.-Y. Xie, C. Li, W.-T. Mi, Y. Yang, and T.-L. Ren, "A graphene-based resistive pressure sensor with record-high sensitivity in a wide pressure range," Sci. Rep. **5**, 8603 (2015).

[10]J. Lee, Z. Wang, K. He, J. Shan, and P. X.-L. Feng, "High frequency MoS$_2$ nanomechanical resonators," ACS Nano **7**, 6086–6091 (2013).

[11]C. Lee, X. Wei, J. W. Kysar, and J. Hone, "Measurement of the elastic properties and intrinsic strength of monolayer graphene," Science **321**, 385–388 (2008).

[12]R. J. Nicholl, H. J. Conley, N. V. Lavrik, I. Vlassiouk, Y. S. Puzyrev, V. P. Sreenivas, S. T. Pantelides, and K. I. Bolotin, "The effect of intrinsic crumpling on the mechanics of free-standing graphene," Nat. Commun. **6**, 8789 (2015).

[13]A. Zandiatashbar, G.-H. Lee, S. J. An, S. Lee, N. Mathew, M. Terrones, T. Hayashi, C. R. Picu, J. Hone, and N. Koratkar, "Effect of defects on the intrinsic strength and stiffness of graphene," Nat. Commun. **5**, 3186 (2014).

[14]S. Deng and V. Berry, "Wrinkled, rippled and crumpled graphene: An overview of formation mechanism, electronic properties, and applications," Mater. Today **19**, 197–212 (2016).

[15]M. Huang and J. R. Greer, "Measuring graphene piezoresistance via in-situ nanoindentation," ECS Trans. **35**, 211–216 (2011).

[16]C. Wong, M. Annamalai, Z. Wang, and M. Palaniapan, "Characterization of nanomechanical graphene drum structures," J. Micromech. Microeng. **20**, 115029 (2010).

[17]D. Davidovikj, F. Alijani, S. J. Cartamil-Bueno, H. S. van der Zant, M. Amabili, and P. G. Steeneken, "Nonlinear dynamic characterization of two-dimensional materials," Nat. Commun. **8**, 1253 (2017).

[18]R. Lifshitz and M. Cross, "Nonlinear dynamics of nanomechanical and micromechanical resonators," Rev. Nonlinear Dyn. Complexity **1**, 1–52 (2008).

[19]J. Atalaya, A. Isacsson, and J. M. Kinaret, "Continuum elastic modeling of graphene resonators," Nano Lett. **8**, 4196–4200 (2008).

[20]Z. Wang and P. X.-L. Feng, "Dynamic range of atomically thin vibrating nanomechanical resonators," Appl. Phys. Lett. **104**, 103109 (2014).

[21]C. Chen, S. Lee, V. V. Deshpande, G.-H. Lee, M. Lekas, K. Shepard, and J. Hone, "Graphene mechanical oscillators with tunable frequency," Nat. Nanotechnol. **8**, 923–927 (2013).

[22]D. I. Caruntu and I. Alvarado, "On electrostatically actuated NEMS/MEMS circular plates," Proc. SPIE **7981**, 79810Z (2011).

[23]A. W. Leissa and M. S. Qatu, *Vibrations of Continuous Systems* (McGraw-Hill, 2011).

[24]A. Eriksson, D. Midtvedt, A. Croy, and A. Isacsson, "Frequency tuning, nonlinearities and mode coupling in circular mechanical graphene resonators," Nanotechnology **24**, 395702 (2013).

[25]C. Chen, *Graphene NanoElectroMechanical Resonators and Oscillators* (Columbia University, 2013).

[26]A. Castellanos-Gomez, M. Buscema, R. Molenaar, V. Singh, L. Janssen, H. S. van der Zant, and G. A. Steele, "Deterministic transfer of two-dimensional materials by all-dry viscoelastic stamping," 2D Mater. **1**, 011002 (2014).

[27]B. Arash and Q. Wang, "Vibration of single-and double-layered graphene sheets," J. Nanotechnol. Eng. Med. **2**, 011012 (2011).

[28]M. Amabili, F. Alijani, and J. Delannoy, "Damping for large-amplitude vibrations of plates and curved panels, part 2: Identification and comparisons," Int. J. Non-Linear Mech. **85**, 226–240 (2016).

[29]S. Timoshenko, S. Woinowsky-Krieger, and S. Woinowsky, *Theory of Plates and Shells* (McGraw-Hill, New York, 1959), Vol. 2.

[30]W.-M. Zhang, H. Yan, Z.-K. Peng, and G. Meng, "Electrostatic pull-in instability in MEMS/NEMS: A review," Sens. Actuators, A **214**, 187–218 (2014).

[31]J. Xia, F. Chen, J. Li, and N. Tao, "Measurement of the quantum capacitance of graphene," Nat. Nanotechnol. **4**, 505–509 (2009).

[32]C. Zhan, J. Neal, J. Wu, and D.-E. Jiang, "Quantum effects on the capacitance of graphene-based electrodes," J. Phys. Chem. C **119**, 22297–22303 (2015).

[33]E. J. Doedel, A. R. Champneys, T. F. Fairgrieve, Y. A. Kuznetsov, B. Sandstede, and X. Wang, Auto97, 1998.

[34]J. Guckenheimer and P. J. Holmes, *Nonlinear Oscillations, Dynamical Systems, and Bifurcations of Vector Fields* (Springer Science and Business Media, 2013), Vol. 42.

[35]D. J. Inman, *Engineering Vibration* (Pearson, Saddle River, NJ, 2014).

[36]D. J. Ewins, *Modal Testing: Theory and Practice* (Research Studies Press, Letchworth, 1984), Vol. 15.

[37]J. Xiao and J. Gillespie, Jr., *Fracture Behaviors of Graphene Sheets and Carbon Nanotubes* (InTech Open Access Publisher, 2011).

[38]A. Isacsson, A. W. Cummings, L. Colombo, L. Colombo, J. M. Kinaret, and S. Roche, "Scaling properties of polycrystalline graphene: A review," 2D Mater. **4**, 012002 (2016).

[39]A. Shekhawat and R. O. Ritchie, "Toughness and strength of nanocrystalline graphene," Nat. Commun. **7**, 10546 (2016).